Journal Pre-proofs

On the fatigue properties of a third generation aluminium-steel butt weld made by hybrid metal extrusion & bonding (HYB)

Lise Sandnes, Torgeir Welo, Øystein Grong, Filippo Berto

PII: S0142-1123(21)00435-7
DOI: https://doi.org/10.1016/j.ijfatigue.2021.106586
Reference: JIJF 106586

To appear in: *International Journal of Fatigue*

Received Date: 8 July 2021
Revised Date: 8 September 2021
Accepted Date: 5 October 2021

Please cite this article as: Sandnes, L., Welo, T., Grong, O., Berto, F., On the fatigue properties of a third generation aluminium-steel butt weld made by hybrid metal extrusion & bonding (HYB), *International Journal of Fatigue* (2021), doi: https://doi.org/10.1016/j.ijfatigue.2021.106586

On the fatigue properties of a third generation aluminium-steel butt weld made by hybrid metal extrusion & bonding (HYB)

Lise Sandnes*[,a], Torgeir Welo[a], Øystein Grong[a,b], Filippo Berto[a]

[a]Department of Mechanical and Industrial Engineering, Norwegian University of Science and Technology (NTNU), Richard Birkelands vei 2b, 7491 Trondheim, Norway

[b]HyBond AS, NAPIC, Richard Birkelands vei 2b, 7491 Trondheim, Norway

*Corresponding author: E-mail address: lise.sandnes@ntnu.no

Abstract

The present investigation is concerned with the high-cycle axial fatigue behaviour of a third generation Al-steel butt weld made by hybrid metal extrusion & bonding (HYB). In this particular weld, metallurgical bonding is achieved by a combination of microscale mechanical interlocking and intermetallic compound (IMC) formation, where the IMC layer is in the sub-micrometre range (< 1μm). During high-cycle fatigue testing this microstructure provides a high intrinsic resistance against interfacial cracking. In the as-welded condition, fatigue fracture typically initiates at the weld toe on the aluminium side of the joint due to the unfavourable effect of having a geometrical stress riser localised inside the soft heat-affected zone. Since the interfacial bond strength is not a limiting factor, the fatigue properties of the Al-steel HYB butt weld are seen to fully match those of corresponding Al-Al weldments produced by gas metal arc welding, laser beam welding and friction stir welding.

Keywords: *Solid-state welding; hybrid metal extrusion & bonding (HYB); aluminium-steel butt welding; high cycle fatigue; S-N curves.*

Nomenclature

A	Curve-fitting constant
Al	Aluminium
B	Curve-fitting constant
BM	Base metal
DIC	Digital image correlation
E	Elastic modulus
FE	Finite element
FM	Filler metal
F_{max}	Maximum force
F_{min}	Minimum force
FW	Filler wire
HAZ	Heat-affected zone
HYB	Hybrid Metal Extrusion & Bonding
IMC	Intermetallic compound
K	Strength index
n	Strain hardening exponent
N_f	Number of cycles to failure
r^2	Correlation coefficient
R	Loading ratio
RT	Room temperature
SEM	Scanning electron microscope
t	Thickness
w	Width
Δσ	Stress range
ε_{eng}	Engineering strain
ε_f	Fracture strain
ε_p	True plastic strain
σ_{el}	Elastic limit
σ_{eng}	Engineering stress
σ_p	True plastic stress
σ_{UTS}	Ultimate tensile strength

σ_{ys}	Yield strength
$\hat{\sigma}$	Sampling variance
v	Poisson's ratio

1 Introduction

Today's automotive design relies heavily on the use of mixed-materials solutions, promoting weight reductions and manufacturing of eco-friendly vehicles with enhanced performance and functionality [1-4]. This creates a demand for improved multi-material joining methods that can compete with and eventually replace existing ones [3-7]. However, because the requirements of the resulting joint integrity are very stringent, considerable benchmark testing and documentation are needed before a new, innovative process will be adopted and used in production in the automotive industry [8].

Considering aluminium (Al)-steel welding, which is the focus area of the present study, benchmarking is usually done against well-proven commercial methods such as gas tungsten arc welding (GTAW), gas metal arc welding (GMAW), pulsed GMAW (PGMAW), laser beam welding (LBW), cold metal transfer welding (CMTW) and friction stir welding (FSW), either used separately or in combination [6, 7, 9-34]. All these processes have in common that they enable metallurgical bonding via intermetallic compound (IMC) formation [9, 35-37]. However, since IMCs, in general, are both hard and brittle, many Al-steel welds will be prone to interfacial cracking and consequently display low yield and tensile strengths during tensile loading [13, 14, 23, 31-33, 38-46]. Still, low-heat input methods, like FSW and CMTW, can be used to produce Al-steel welds with sufficient static strength to make them suitable for automotive applications [16, 47]. This is because the low process temperature reduces the risk of excessive growth of the IMC interface layer during welding [48].

Hybrid Metal Extrusion & Bonding (HYB) is a relatively new solid-state joining method for metals and alloys. The HYB method, which is based on the principles of continuous extrusion, utilizes aluminium filler metal (Al-FM) additions in combination with severe plastic deformation of the base and filler metals to consolidate the joint [49, 50]. Although the original idea was to use HYB only for welding of aluminium alloys, the method has evolved into a

multi-material joining process capable of handling a wide range of base metal combinations (Al, Fe, Ti and Cu) [49, 51-58]. Recently, its potential for butt welding of 4 mm thick plates of AA6082-T6 and S355 structural steel has been demonstrated [59-61]. For example, the third generation Al-steel HYB butt weld reveals tensile strength values up to 266 MPa in the as-welded condition [61]. This is due to its favourable interface microstructure, which prevents cracking along the bond line during tensile loading [61]. As a result, all plastic deformations throughout necking and final fracture occur in the heat-affected zone (HAZ) on the aluminium side of the joint, while the steel part remains within the elastic regime [61]. This favourable deformation mode has also been observed in conventional Al-steel butt joints made by CMTW and FSW [16, 62-67]. However, in most of these cases, a soft aluminium base metal (Al-BM) is used in combination with structural steel [16, 62-66]. Hence, the tensile properties of the third generation Al-steel HYB butt weld surpass those reported for comparable friction stir welds [61].

Interfacial cracking is also a serious problem in fatigue testing of Al-steel welds, particularly if the welds are encumbered with defects like root and surface cracks or suffer from the lack of bonding. This undesirable fracture behaviour is typical for Al-steel lap and spot welds [68-77] as well as Al-steel butt welds [63, 78, 79]. In the latter case, it is therefore necessary to use machined or polished specimens to remove visible flaws and surface imperfections prior to fatigue testing in order to obtain consistent and reproducible results [63, 78, 79]. Still, even under such idealised conditions, final fracture usually occurs along the IMC layer at the Al-steel interface [63, 78, 79]. This substantiates the important role that the interface microstructure plays in the fatigue behaviour of Al-steel welds.

Therefore, it would be of interest to put the third generation Al-steel HYB butt weld to the test and check out whether the combination of microscale mechanical interlocking and IMC formation provides a bond strength that is sufficient to prevent interfacial cracking during

cyclic tensile loading. Accordingly, the main objective of the present work is to evaluate the fatigue properties of the third generation Al-steel HYB weld, with the main emphasis on its macrostructural characteristics. This will be achieved by conducting high-cycle axial fatigue testing of as-welded specimens, along with optical microscope examinations of the joint cross-section and scanning electron microscope (SEM) examinations of selected fracture surfaces to reveal the crack initiation points. In addition, dedicated finite element (FE) simulations will be conducted to identify the geometrical stress risers that trigger fatigue crack initiation in the HYB joint upon tensile loading. Finally, due to the lack of validated literature data for as-welded Al-steel butt welds, the fatigue properties will be benchmarked against corresponding data reported for comparable Al-Al butt welds produced using conventional welding techniques. Based on these examinations, new insights into how Al-steel butt welds with optimised bond strength behave under fatigue loading have been obtained.

The remaining parts of this paper are structured as follows. First, an overview of the experimental set-up, test procedure and FE modelling will be given. Then, the main results from the fatigue testing and fractographic examination are presented, followed by a discussion of the main findings. Finally, the main conclusions will be given.

2 Method

2.1 Materials, welding conditions and joint properties

The Al-steel butt joint selected for the fatigue testing is identical to the 4 mm thick third generation Al-steel HYB butt weld referred to in the introduction. Since details of the applied experimental set-up and welding conditions used to fabricate the joint have been reported elsewhere [61], only a brief summary is given below along with some additional information about its interface microstructure and tensile properties.

Figure 1 shows a schematic drawing of the experimental set-up used in the welding trial. Included is also a sketch of the HYB PinPoint extruder, highlighting its core parts. As a starting point, the two 4 mm thick base plates are first mounted in a fixture so that a 3 mm wide I-groove forms between them. The plates rest again on a grooved steel backing to facilitate the formation of a shaped root crown. The Ø7 mm rotating pin tip is then submerged into the groove while being accurately positioned to make sure that it barely touches the steel groove wall during welding without machining it. The pin itself is provided with four moving dies. This allows the Al-FM to flow into the groove below in a continuous manner as soon as the aluminium filler wire (Al-FW) hits the abutment and the pressure build-up in front becomes sufficiently high to initiate extrusion. In this set-up, the stationary housing is also equipped with a separate die opening at the rear for partial outlet of the extrudate. This means that a shaped weld reinforcement will form on the top of the joint. Further details about the HYB PinPoint extruder and its tool parts can be found elsewhere [49, 50, 80].

During butt welding the HYB PinPoint extruder with its submerged rotating pin tip slides along the joint line at constant speed and continuously fills the entire weld groove with solid aluminium in one pass [49, 54]. The specific operational conditions employed in the manufacturing of the third generation Al-steel HYB butt weld are summarised in **Table 1**. **Table 2** and **Table 3** list the chemical compositions of the Al-FW, the aluminium base metal (Al-BM) and the steel base metal (S-BM).

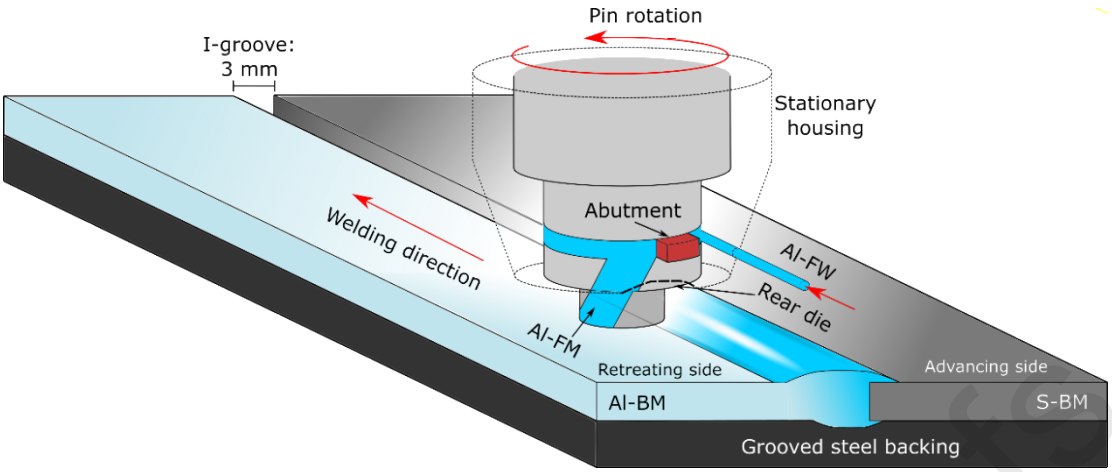

Figure 1 *Schematic illustrations of the HYB PinPoint extruder and experimental set-up used in the manufacturing of the third generation Al-steel HYB butt weld.*

Table 1 *Operational conditions employed in the manufacturing of the third generation Al-steel HYB butt weld [61].*

Pin rotation (RPM)	Travel speed (mm/s)	Wire feed rate (mm/s)	Groove width (mm)	Gross heat input (kJ/mm)
400	9	155	3	0.30

Table 2 *Chemical composition (in wt.%) of the rolled AA6082-T6 base metal (Al-BM) and the Ø1.4 mm AA6082-T4 filler wire (Al-FW) used in the manufacturing of the third generation Al-steel HYB butt weld [61].*

Material	Si	Mg	Fe	Cu	Mn	Cr	Zn	Ti	Zr	B	Others	Al
Al-BM	1.21	0.71	0.24	0.06	0.59	0.04	0.04	0.020	-	-	0.150	Balance
Al-FW	1.11	0.61	0.20	0.002	0.51	0.14	-	0.043	0.13	0.006	0.029	Balance

Table 3 *Chemical composition (in wt.%) of the rolled S355 steel base metal (S-BM) used in the manufacturing of the third generation Al-steel HYB butt weld [61].*

Material	C	Si	Mn	P	S	Cr	Ni	Cu	Al	Nb	B	N	Fe
S-BM	0.056	0.01	0.46	0.009	0.003	0.02	0.04	0.01	0.041	0.006	0.0001	0.003	Balance

A macrograph of the transverse cross-section of the 4 mm thick Al-steel HYB butt weld is shown in **Figure 2**(a). Because the steel plate is located on the advancing side (AS), the down-flow of the Al-FM from the upper part of the groove towards the root region will be most

extensive along the Al-steel interface, as illustrated by the white arrows in the image. This provides favourable conditions for metallurgical bonding by IMC formation. In fact, the rotating pin tip-steel groove wall interaction is so severe that the Al-steel interface becomes wavy because of scribing, as shown by the SEM backscatter electron image in **Figure 2**(b). This gives additional bond strengthening through mechanical interlocking [53, 60, 61]. At the same time the IMC layer is seen to be in the sub-micrometre range (< 1µm), indicating high intrinsic resistance against cracking during tensile loading [61]. On the retreating side (RS), the material flow is dominated by the rotating action of the pin. Hence, the Al-BM will be dragged along with the pin and subsequently deposited in the groove behind, as indicated by the black arrow in **Figure 2**(a). In the HYB case, metallic bonding between the Al-FM and the Al-BM is achieved through a combination of oxide dispersion, shear deformation, surface expansion and pressure [53, 54].

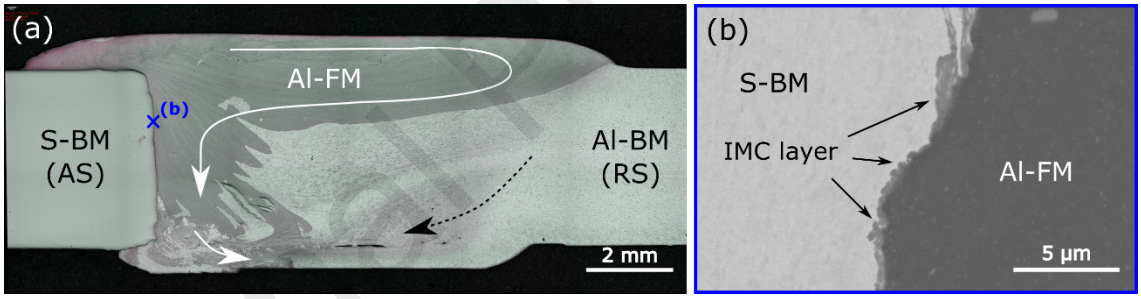

Figure 2 *Metallographic characterisation of the third generation Al-steel HYB butt weld; (a) Macrograph of a transverse section of the joint and (b) SEM backscatter electron image of the Al-steel interface at the position indicated in (a).*

Table 4 summarises the measured yield strength (σ_{ys}), tensile strength (σ_{UTS}) and fracture strain (ε_f) of the third generation Al-steel HYB butt weld tested in the as-welded condition [61]. Included are also the corresponding mechanical properties of the aluminium and steel base metals. It has previously been shown that the tensile strength of the Al-steel HYB butt joint

exceeds most comparable Al-steel butt welds made using conventional welding techniques, including FSW [61].

Table 4 *Summary of the measured yield strengths (σ_{ys}), tensile strengths (σ_{UTS}) and fracture strains (ε_f) of the Al-steel HYB butt weld ($HYB_{Al\text{-}steel}$), the AA6082-T6 base metal (Al-BM) and the S355 steel base metal (S-BM) [61].*

Property	$HYB_{Al\text{-}steel}$	Al-BM	S-BM
σ_{ys} $[MPa]$	198	325	412
σ_{UTS} $[MPa]$	266	349	498
ε_f [%]	7	14	28

2.2 Fatigue testing

Figure 3 shows a photograph (top view) of the entire Al-steel HYB butt weld, where the approximate locations of the fatigue specimens used in the present study are indicated. They are labelled F1 through F12 from left to right in the image. The other parts of the weld have previously been used for tensile testing and microscope examinations, as reported in Ref. [61].

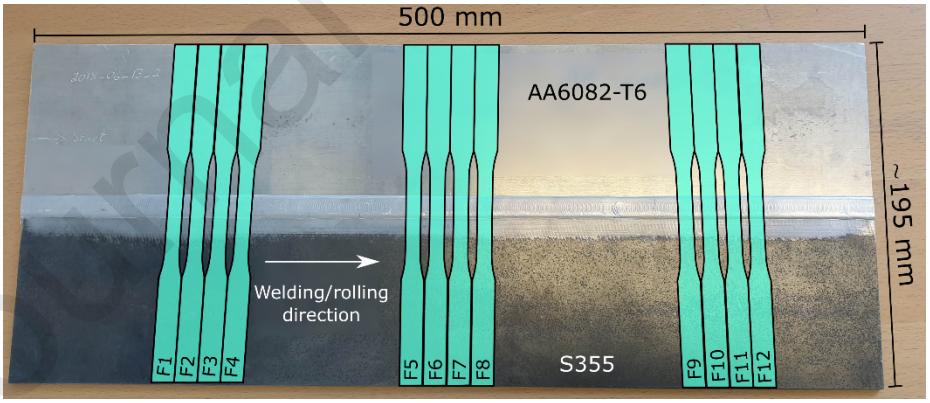

Figure 3 *Overview of the entire third generation Al-steel HYB butt weld showing the approximate locations and correct labelling of the transverse specimens being used in the fatigue testing. The welding/base plate rolling directions and the total length/width of the butt-welded plates are also indicated in the image.*

At present, no standard test method exists for fatigue testing of dissimilar material weldments. Therefore, the transverse fatigue test specimens were prepared in accordance with ASTM

standard E466-15 [81]. In the present case, however, the specimen's parallel length was extended to 40 mm to make sure the entire soft zone on the aluminium side of the joint was captured by the sampling area. All specimens had their centre located in the middle of the weld. In total twelve fatigue specimens sampling different regions of the Al-steel HYB butt weld were prepared. In addition, fourteen specimens sampling the T6-heat treated Al-BM were extracted and prepared from a separate base plate. Note that all specimens were tested in either the as-welded or the as-received condition, implying that their surface finish has not been altered by machining or polishing prior to fatigue testing. The dimensions of the fatigue specimens are further highlighted in **Figure 4**.

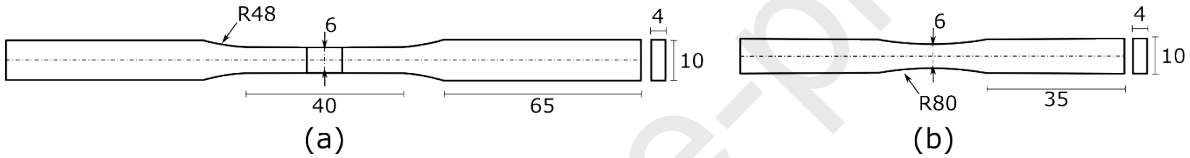

Figure 4 *Schematic drawings showing the shape and dimensions of the fatigue specimens used in the present investigation; (a) the Al-steel HYB butt weld specimens and (b) the Al-BM specimens. All numbers provided are in mm.*

Constant-amplitude axial fatigue tests were carried out using a sinusoidal load-time mode at a fixed stress ratio R of 0.1. The tests were conducted at room temperature (RT), employing an Instron E10000 ElectroPuls electrodynamic test machine provided with a load cell of 10 kN (operating at 30-50 Hz). The fatigue life of the specimens tested was defined as the number of cycles to total fracture at a given stress range. Similarly, in cases where test failure did not occur, the test run-out was set to $2 \cdot 10^6$ cycles. To obtain the desired high-cycle fatigue S-N (stress-life) diagrams, the maximum applied stress level during testing was first set to about 67% of the measured ultimate tensile strength (UTS) for each category of test specimens. Subsequently, the maximum stress level was gradually decreased/increased to obtain data in

the range of $10^4 - 2 \cdot 10^6$ cycles to failure. Details of the applied load and frequency for each individual specimen tested can be found in the Appendix.

2.3 Fractographic examinations

Selected fracture surfaces of broken fatigue specimens were examined in a Quanta FEG 450 scanning electron microscope (SEM) at different magnifications to determine the crack initiation point and the subsequent propagation direction. These fractographic examinations were conducted at an acceleration voltage of 20 kV.

2.4 Finite element simulations

2.4.1 Main purpose

Finite element (FE) simulations of the Al-steel HYB butt weld were conducted to evaluate how factors, such as the upper and lower weld reinforcements in combination with the previously observed HAZ softening, affect the resulting stress distribution during tensile loading. Because the third generation Al-steel HYB butt weld is not prone to interfacial cracking, a simplified approach just focusing on these two aspects is deemed to be sufficient to expose potential geometrical stress risers triggering the fatigue crack initiation in the present HYB joint. Thus, the main purpose of the FE model is to evaluate and quantify the stress distribution in the specimen upon loading.

2.4.2 Modelling

The simulations were done using the commercial finite element (FE) software code ABAQUS/CAE 2017. As a starting point, a full three-dimensional ABAQUS model of the HYB Al-steel fatigue specimens was made, based on inputs from **Figure 2** and **Figure 4**(a) and extended to the third dimension. No fictious radii were used at the weld toes. Furthermore, by assuming perfect bonding across the interface, the Al and steel regions of the weld can be modelled as two individual objects and assembled using tied constrains. The Al part is

modelled as a deformable object presented by a solid mesh of about 510,000 linear brick elements (C3D8R). A finer mesh is chosen at the upper and lower weld toes of the specimen, where most of the plastic deformation occurs due to the HAZ softening. On the other hand, the steel part is modelled as a rigid body, meaning that neither stresses nor strains are calculated. The applied boundary conditions were similar to those deemed prevailing during the experimental fatigue testing, i.e. all six degrees of freedom (DOFs) were fixed in the grip-section of the steel part, whereas the grip-section of the Al part was fixed in five DOFs, allowing displacement in the axial loading direction only. A concentrated tensile load, up to the maximum nominal tensile strength of the welded joint, was applied on the end of the Al region in the FE simulations.

2.4.3 Materials input data

In welded assemblies, local variations in material properties will affect the resulting stress distributions during loading [82]. To capture the effect of steep gradients in the material properties between the different regions, the FE-model of the joint is divided into different material zones. In total, four different material zones are applied in the FE-model, i.e. the Al-FM, HAZ(1), HAZ(2) and the unaffected Al-BM, as shown in **Figure 5**. The sub-division is done on the basis of the optical image of the weld zone shown in **Figure 2** as well as on inputs from the previous digital image correlation (DIC) analysis of the deformation behaviour of the same joint during tensile testing [61]. The DIC data called for employing two different HAZ regions to allow the important softening effect to be captured in an adequate manner.

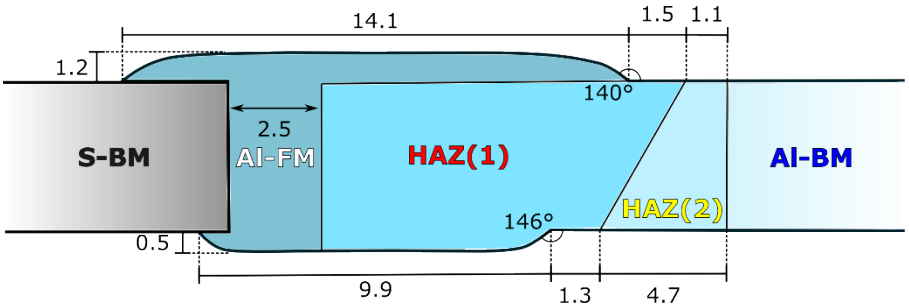

Figure 5 *Sketch of the transverse section of the modelled fatigue specimen showing the geometry of the weld reinforcements and the sub-division of the HYB weld into different material zones. The weld toe angles are provided in degrees, while all other numbers are provided in mm.*

In the FE-model, relevant material input data are needed for each material zone. Since the S-BM is treated as a rigid body, no material properties are assigned to this section. The required true stress-true strain input data for both the Al-BM, the Al-FM, the HAZ(1) and the HAZ(2) have been obtained from three different sources [56, 61, 83]. In the ABAQUS model, the initial yield surface is assumed to be isotropic and display isotropic work hardening. The elastic limit, σ_{el}, corresponds to the load where the material response starts to deviate from the linear behaviour, sometimes referred to as the 0.01% offset proof stress in the literature [84]. In the present case, σ_{el} is determined based on a semi-quantitative analysis of the reported stress-strain data. In the plastic regime, the isotropic work hardening behaviour is captured by fitting the true stress-true strain curves to Ludwiks' law [85]:

$$\sigma_p = K(\varepsilon_p)^n \qquad (1)$$

where σ_p is the true plastic stress, ε_p is the true plastic strain, while K is the strength index, and n is the strain hardening exponent. **Table 5** summarizes the main material input data used in the FE-model, including the relevant values for σ_{el}, K and n for the different material zones in question.

Table 5 *Summary of the material input data used in the FE-model to capture the deformation behaviour of the 6082-T6 aluminium base metal (Al-BM), the 6082-T4 aluminium filler metal (Al-FM) and the HAZ(1) and HAZ(2) materials. Here E is the elastic modulus, v is the Poisson's ratio, σ_{el} is the elastic limit, whereas K and n are the material parameters in Ludwik's law.*

	E **[MPa]**	***v***	$\boldsymbol{\sigma_{el}}$ **[MPa]**	***K*** **[MPa]**	***n***	**Source**
Al-BM	70000	0.33	290	266.1	0.4989	[83]
Al-FM			177	407.4	0.5998	[56]
HAZ(1)			150	375.0	0.4910	[61]
HAZ(2)			170	351.9	0.4772	[61]

3 Results

3.1 Response of Al-steel HYB butt weld and Al base metal to axial fatigue loading

As a starting point, all specimens were visually examined before they were subjected to fatigue testing. The specimens were found to be free from macroscopic flaws like root cracks and surface defects. However, one of the specimens (i.e. specimen F4) contained visible cracks in the weld root region prior to testing, which is deemed to affect the resulting fatigue properties.

The main results from the fatigue testing of the Al-steel HYB butt weld and the Al-BM are summarized in **Figure 6** (see Appendix for original fatigue test data). Included in this double logarithmic S-N (stress-life) diagram are both the measured fatigue data for specimens that failed during testing, the run-out data (denoted by black arrows), the best-fit linear regression line (i.e. mean S-N curve) and the 95% confidence band of the mean curve for the two data sets in question. The linear regression analysis was conducted in accordance to ASTM standard E739-10 [86], where the mean S-N curve is presented on the form:

$$\log_{10} N_f = A + B \cdot \log_{10} \Delta\sigma \qquad (2)$$

where N_f is the number of cycles to failure, $\Delta\sigma$ is the stress range of the applied amplitude, while A and B are curve-fitting constants. Note that neither the data point in brackets, which

represent specimen F4 containing visible root defects prior to testing, nor the run-out data are included in the regression analysis. **Table 6** summarises the calculated values for the constants A and B in Equation (2) along with the estimated variance $\hat{\sigma}$ of the normal distribution for log N and the correlation coefficient r^2 for the two data sets. Note that the applied sampling procedure (i.e. sample size and tests replicability) is in accordance with that required by ASTM standard E739-10(2015) for research and development testing of components and specimens [86].

It is evident from **Figure 6** and **Table 6** that the fatigue properties of the Al-steel HYB butt weld are significantly lower than those of the Al-BM. This is similar to that observed during fatigue testing of welded components in general [87]. Moreover, a closer inspection of **Figure 6** reveals that the spread in data is relatively low, as indicated by the estimated variance of the normal distributions and the calculated values for the correlation coefficients in **Table 6**. Hence, the present HYB joint yields consistent and reproducible results in the as-welded condition.

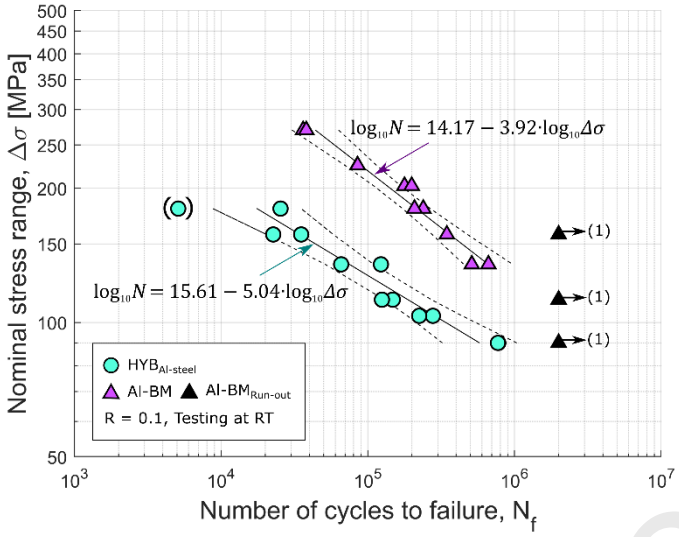

Figure 6 *Summary of the results from the fatigue testing of the Al-steel HYB butt weld ($HYB_{Al\text{-}steel}$) and the aluminium base metal (Al-BM). Included is also the calculated mean S-N curve and the corresponding 95 % confidence band for each data set.*

Table 6 *Summary of the results from the linear regression analysis of the fatigue data presented in* ***Figure 6****, where A and B are constants, $\hat{\sigma}$ is the estimated variance of the normal distribution for log N and r^2 is the calculated correlation coefficient.*

Type of specimen	*A*	*B*	$\hat{\sigma}$	r^2
Al-BM	14.17	-3.92	0.0877	0.961
$HYB_{Al\text{-}steel}$	15.61	-5.04	0.1467	0.932

3.2 Fracture analysis

After fatigue testing, all specimens were visually examined. **Figure 7**(a) and (b) show the resulting fracture location of two representative specimens (i.e. F5 and F10) being extracted from the central and end region of the butt weld, respectively. As can be seen from the photographs, final failure typically occurs at the weld toe on the aluminium side of the joint. This failure mode is representative of ten out of twelve specimens tested. For specimen F4, which contained large visible cracks in the root region prior to testing, the final fracture is seen to run close to the Al-steel interface, as shown in **Figure 7**(c). This is not surprising,

considering the previously mentioned devastating effect that defects have on the fatigue life of Al-steel welds. In addition, one specimen (i.e. F3) did fracture in the central part of the weld; i.e. inside the so-called extrusion zone (EZ), as can be seen from **Figure 7**(d).

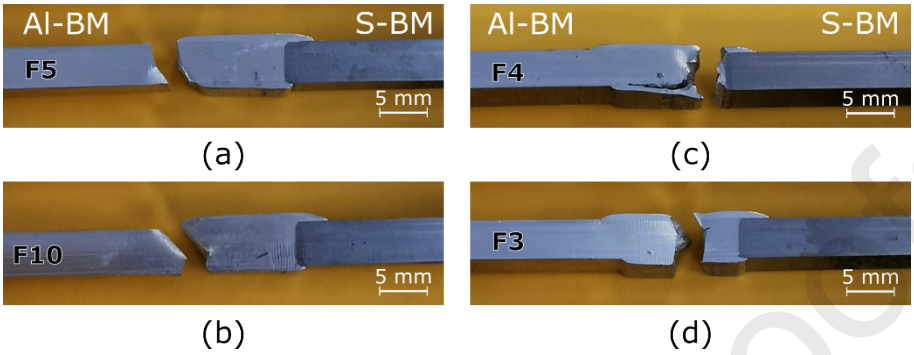

Figure 7 *Photographs revealing the fracture path of selected specimens following fatigue testing; (a) specimen F5, (b) specimen F10, (c) specimen F4 and (d) specimen F3.*

After visual examination, selected fracture surfaces were examined in the SEM in order to determine the fatigue crack initiation points. **Figure 8**(a) and (b) show low magnification fractographs, revealing the entire fracture surface of the two previously selected specimens F5 and F10 located in the central and end region of the butt weld, respectively. As can be seen from **Figure 8**(a), which refers to specimen F5, the fatigue crack initiates at the weld face. In contrast, the crack initiation in specimen F10, which is located at the end of the weld, started in the weld root region, as shown in **Figure 8**(b). This initiation mode is representative of nine out of twelve specimens tested, including specimen F3, which fractured inside the EZ (see **Figure 8**(c)). Hence, just three of the specimens (i.e. F1, F2 and F5) did reveal fatigue crack initiation at the weld face.

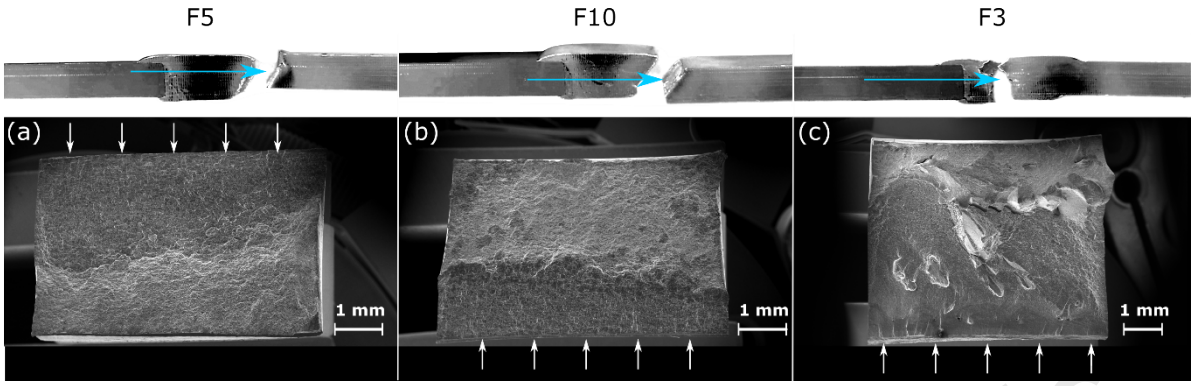

Figure 8 *SEM images of selected fracture surfaces of broken fatigue specimens taken from different parts the Al-steel HYB butt weld; (a) specimen F5 tested at a stress range of 112 MPa, (b) specimen F10 tested at a stress range of 160 MPa and (c) specimen F3 tested at a stress range of 135 MPa. Blue arrows point towards the fracture surfaces being examined, while white arrows indicate the fatigue crack initiation point in each case.*

4 Discussion

4.1 Finite element analysis

As a starting point, the FE model is validated against the static experimental stress-strain curve for the third generation Al-steel HYB butt weld, which is based on the tensile test results and the DIC data reported in the previous study [61]. **Figure 9** shows a comparison between the measured (solid line) and simulated (dashed line) engineering stress-strain curves. Note that, in both cases, the measuring area was 15 mm, extending from the Al-steel interface to the unaffected Al-BM as indicated by the sketch in the lower part of **Figure 9**. It follows that the FE model gives a fair representation of the mechanical response during tensile loading. This indicates that the simulation set-up is sound and that the applied input data and boundary conditions are reasonable in the context of the model being developed. Furthermore, the comparison shows that the simplified stress-strain model used in the FE analysis also provides a good representation of the uniaxial case. Hence, the FE model is deemed to be sufficiently relevant and comprehensive to be used in the more detailed forthcoming analyses of the local stress risers that trigger the fatigue crack initiation in the present HYB joint.

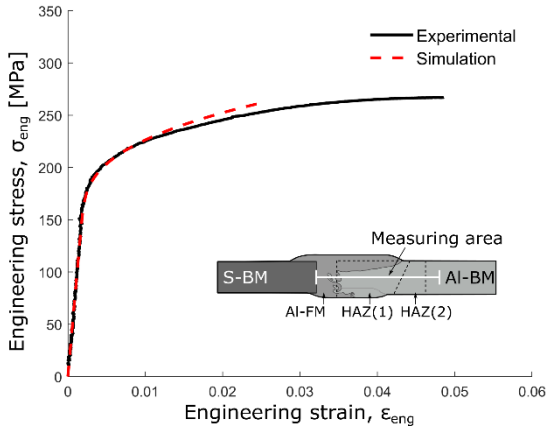

Figure 9 *Comparison between simulated (dashed line) and measured (solid line) engineering stress-strain curves for the third generation Al-steel HYB butt weld. Included is also a sketch showing the location of the measuring area used to extract the two stress-strain curves.*

During the experimental fatigue testing, the applied maximum nominal stress was typically in the range of 100 to 175 MPa. Therefore, in the FE model, a tensile load up-to 175 MPa was simulated to render the first peak load reached during fatigue testing. **Figure 10**(a) and (b) show contour plots of the calculated stress distribution in the Al-steel HYB butt weld at a maximum nominal stress of 150 MPa and 100 MPa, respectively. These values fall within the central and lower part of the S-N (stress-life) diagram (see **Figure 6**). As expected, the two weld reinforcements give rise to a non-uniform stress distribution in the butt weld at both nominal stress levels, acting as stress risers. In particular, at a nominal stress of 150 MPa considerable stress accumulation occurs in the upper part of the joint, as shown in **Figure 10**(a). This highly stressed region is seen to extend far into the gauge section of the fatigue specimen on the aluminium side of the weld. It is believed that the non-uniform stress accumulation, which reflects the somewhat eccentric joint geometry, sets up an internal bending moment in the fatigue specimen upon tensile loading. For the tests conducted at the lower maximum nominal stress level, the stresses in the gauge section seem to be more evenly distributed through the specimen's cross section, as shown in **Figure 10**(b). Hence, a higher stress ratio

(i.e. the local stress at the weld toes *vs.* the nominal stress in the gauge section) is generated at the lower stress level of 100 MPa. Moreover, as can be seen from **Figure 10**, even though the nominal stress level in the gauge section is below σ_{el}, the material will exceed this stress level locally.

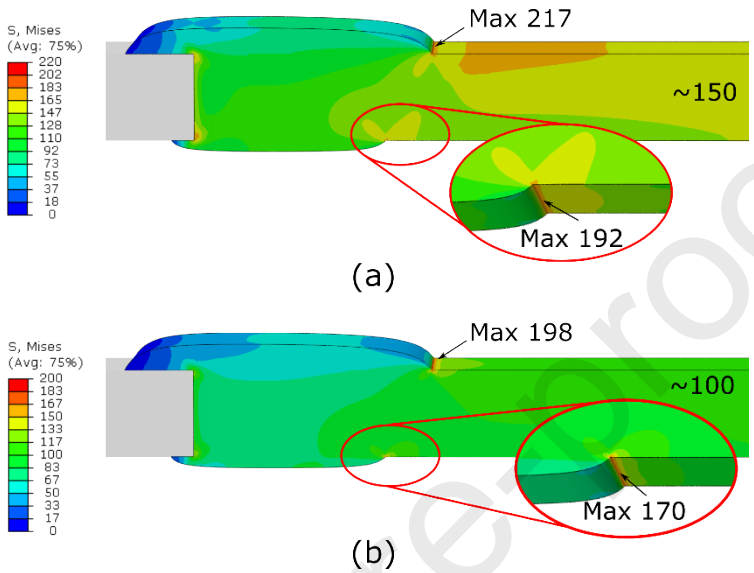

Figure 10 *Calculated von Mises stress distribution in the third generation Al-steel HYB butt weld during tensile loading at a maximum nominal stress level of; (a) 150 MPa and (b) 100 MPa. All values provided are in MPa.*

Although considerable stresses develop in the HYB joint during testing, the FE model reveals that neither a maximum nominal stress of 150 MPa nor 100 MPa lead to global plastic deformations in the gauge section of the fatigue specimen, as shown in **Figure 11**. This is also true for the applied maximum nominal stress of 175 MPa (not shown here). However, plastic strains accumulate locally at the upper and lower weld toes due to HAZ softening. The accumulated plastic strain concentration is significantly higher at a nominal stress level of 150 MPa (see **Figure 11**(a)), yet also noticeable at 100 MPa (see **Figure 11**(b)). This shows the unfavourable effect of having a geometrical stress riser like a reinforcement inside a soft HAZ from a fatigue point of view.

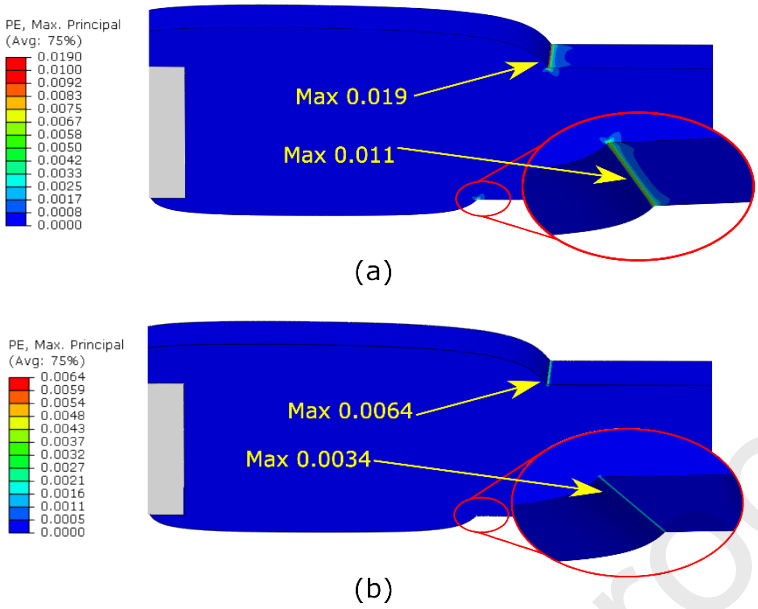

Figure 11 *Calculated values for the accumulated plastic strain in the third generation Al-steel HYB butt weld during tensile loading at a maximum nominal stress level of; (a) 150 MPa and (b) 100 MPa. Note the pertinent difference in scale magnitude between (a) and (b).*

4.2 Origin of fatigue failure

In testing of mono-metallic weldments, it is generally accepted that geometrical discontinuities such as a weld reinforcement will have a negative effect on the resulting fatigue properties [87-91]. Since the mechanical integrity of the third generation Al-steel butt weld is not compromised by bonding defects or reduced bond strength, it has a high intrinsic resistance to interfacial cracking. Still, its fatigue strength is well below that of the AA6082-T6 base metal, as shown previously in **Figure 6**. Obviously, this has to do with the plastic strain accumulation that occurs both at the upper and lower weld toes during fatigue testing due to accompanying HAZ softening. This follows from the FE simulation results presented in **Figure 11**.

Moreover, the fracture analysis of the third generation Al-steel HYB butt weld reveals that fatigue failure mainly initiates at the weld toe in the root region. Only three out of twelve specimens did fail at the upper weld toe. The subsequent examination of the joint geometry of the fractured fatigue specimens disclosed that, in most cases, the root angle was slightly sharper

than that of the weld face angle. This means that the stress ratio is higher in the weld root region, which can explain why fatigue crack initiation typically starts here [89]. In contrast, the FE analysis indicates that the upper weld toe is the weaker part of the joint. However, because the FE model represents an idealised joint geometry, it does not capture local variations in the weld toe radii along the joint line. Hence, many of the fatigue specimens being selected for testing will display the highest stress level in the root region, although this does not show up in the simulations.

4.3 Benchmarking against validated literature data

As already stated in the introduction, interfacial cracking is a serious problem in fatigue testing of Al-steel welds, particularly if the welds are encumbered with flaws like root and surface cracks or suffer from the lack of bonding. Therefore, in the butt welding case testing is instead done on machined or polished specimens, and not on as-welded specimens [63, 78, 79].

Due to the lack of validated literature data for as-welded Al-steel butt welds, the fatigue properties will instead be benchmarked against corresponding data for comparable Al-Al butt welds produced using conventional welding techniques like GMAW, LBW and FSW. This is permissible, since the third generation Al-steel HYB butt weld responds similarly to that of a generic (mono-metallic) aluminium weld during tensile loading.

Table 7 summarises the literature data collected for the benchmarking. These data are presented in the same format as those used for the Al-steel HYB weld shown in **Table 6** in order to enable a direct comparison between the different weldments. Specifically, the data processing procedure involved fitting of the reported S–N curves to Equation (2). Subsequently, the linearised curves are plotted in the range of the original test data. The results are presented graphically in **Figure 12**, together with the Eurocode 9 design curve for Al-Al butt welds (i.e. detail category 45-4.3) [87]. Note that Eurocode 9 curve is based on the 97.7% specific probability of survival, whereas the other curves represent the mean regression line.

Hence, the Eurocode curve is also valid for a higher survival probability than the other ones in **Figure 12** [87]. Although the applied testing conditions are not exactly the same, it is evident from **Figure 12** that the fatigue properties of the third generation Al-steel HYB butt weld in most cases exceed those reported for corresponding generic (mono-metallic) aluminium butt welds, including the Eurocode 9 design curve. Only the 4 mm thick two-pass AA6082-T6 friction stir butt weld is seen to perform slightly better. This is somewhat surprising, considering the fact the Al-steel HYB weld also is provided with two reinforcements acting as stress risers during fatigue testing. Therefore, if the upper and lower surfaces of the Al-steel HYB butt weld instead had been slick like a genuine friction stir weld (which could be achieved through a modification of the tool design), its fatigue properties could potentially have been even better. Therefore, more research is necessary to test the ultimate potential of the HYB process and to optimise the fatigue strength of Al-steel HYB butt welds.

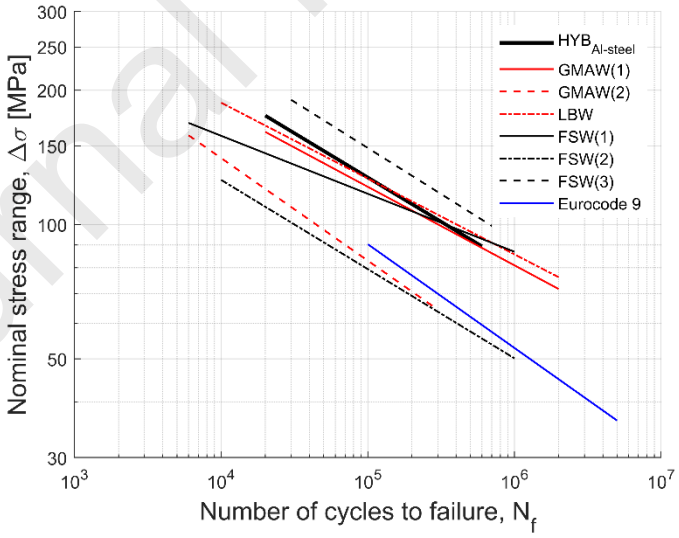

Figure 12 *Master plot showing a comparison between the mean S-N curve for the third generation Al-steel HYB butt weld and those of comparable generic (mono-metallic) aluminium butt welds produced using conventional welding techniques. These curves have been constructed on the basis of Equation (2) and input*

*data from **Table 7**. Note that the Eurocode 9 design curve is also valid for a higher survival probability than the other mean curves in the figure.*

***Table 7** Summary of processed fatigue data for comparable generic aluminium butt welds tested in the as-welded condition and produced using gas metal arc welding (GMAW), laser beam welding (LBW) and friction stir welding (FSW). Note that the data presented represent the mean S-N curves (i.e. 50% survival) for all welds.*

Process	Material	Thickness	UTS_{weld} (MPa)	UTS_{BM} (MPa)	R-ratio	No. of data	*A*	*B*	Source
GMAW(1)	6082-T6	6	221	330	0	8	16.84	-5.68	[92]
GMAW(2)	6082-T6	3	210	323	0.1	16	13.35	-4.35	[93]
LBW	6061-T6	3	265	342	0.1	12	17.37	-5.88	[93]
FSW(1)	6082-T6	3	226	323	0.1	15	20.91	-7.69	[93]
FSW(2)	6082-T6	3	-	320	0.2	7	14.5	-5.00	[94]
FSW(3)	6082-T6	4	241	330	0	25	15.51	-4.84	[95]*

*Double-sided full penetration FS weld.

5 Conclusions

The present work is concerned with high-cycle fatigue testing of a third generation Al-steel butt weld made by Hybrid Metal Extrusion & Bonding (HYB). The main conclusions from this exploratory study can be summarised as follows:

- In the Al-steel HYB butt weld studied, metallurgical bonding is achieved by a combination of microscale mechanical interlocking and intermetallic compound (IMC) formation, where the IMC layer is in the sub-micrometre range (< 1μm). This makes the HYB joint highly resistant against interfacial cracking.
- During fatigue testing at constant stress ratio *R* of 0.1, the 4 mm thick HYB joint responds consistently to cyclic tensile loading within the entire maximum nominal stress range examined, as evidenced by a small spread in the experimental data. Still, the fatigue properties of the Al-steel HYB butt weld are significantly lower than those

of the aluminium base metal (Al-BM). At the same time, the S355 steel base metal (S-BM) remains within the elastic stress region during testing and is thus unaffected by the applied cyclic loading.

- The subsequent fractographic examination of the broken fatigue specimens shows that final fracture typically occurs at the weld toe on the Al-side of the HYB joint. This failure mode is representative of ten out of twelve specimens tested. In only one specimen, which contained large visible cracks in the root region prior to testing, the final fracture ran close to the Al-steel interface.
- Finite element (FE) simulations of the Al-steel HYB butt weld have been conducted to evaluate how factors such as the weld reinforcements in combination with HAZ softening affect the resulting stress distribution during tensile loading. The FE simulations reveal that plastic strains accumulate locally at the upper and lower weld toe due to HAZ softening. The accumulated plastic strain is obviously highest at a high maximum nominal stress level but also noticeable at the lowest stress level being tested. This shows the unfavourable effect of introducing geometrical stress risers, like a reinforcement localised inside a soft HAZ, from a fatigue point of view.
- Due to the lack of validated literature data for as-welded Al-steel butt welds, the fatigue properties of the HYB joint have been benchmarked against corresponding data reported for comparable Al-Al butt welds produced using conventional welding techniques like gas metal arc welding (GMAW), laser beam welding (LBW) and friction stir welding (FSW). The benchmarking shows that the fatigue properties of the third generation Al-steel HYB butt weld in most cases exceed those of the other ones. Only one generic (mono-metallic) AA6082-T6 friction stir butt weld is seen to perform slightly better.

- Since the fatigue properties of the third generation Al-steel HYB butt weld are limited by geometry and reinforcements acting as stress risers, manufacturing of a fourth generation Al-steel HYB butt weld with slick surfaces should be considered to further improve the fatigue strength. This can be achieved through simple modification of the tool design. This suggests that the HYB process has not yet reached its ultimate potential when it comes to optimising the fatigue strength of Al-steel butt welds.

6 Acknowledgements

The authors acknowledge the financial support from HyBond AS, NTNU and NAPIC (NTNU Aluminium Product Innovation Center). They are also indebted to Ulf Roar Aakenes and Tor Austigard of HyBond AS for valuable assistance in producing the Al-steel HYB butt weld examined in the present investigation. Finally, thanks are due to Benetler Aluminium Systems Norway for sharing information on the practical challenges related to aluminium-steel joining.

Appendix

Table A.1 *Summary of the original fatigue test data for the 6082-T6 aluminium base material tested at a constant stress ratio R of 0.1. Here, w and t are the initial width and thickness of the specimen parallel cross-section,* F_{max} *and* F_{min} *are the maximum and minimum force being applied during testing and* N_f *is the number of cycles to failure.*

Specimen nr.	w **(mm)**	t **(mm)**	F_{max} **(N)**	F_{min} **(N)**	**Test frequency (Hz)**	N_f
1	5.97	3.93	3600	360	40	664339
2	5.94	3.93	5400	540	40	177917
3	5.92	3.94	6000	600	40	84862
4	5.97	3.95	7200	720	30	36222
5	5.94	3.94	2400	240	50	Run-out
6	5.96	3.95	7200	720	30	38074
7	5.98	3.95	6000	600	30	85305
8	5.94	3.92	5400	540	40	199158
9	5.96	3.95	4800	480	40	238934
10	5.96	3.94	3600	360	40	511555
11	5.97	3.93	4800	480	40	208198
12	5.93	3.95	3000	300	50	Run-out
13	5.93	3.95	4200	420	50	345857
14	3.95	5.94	4200	420	50	Run-out

Table A.2 *Summary of the original fatigue test data for the Al-steel HYB butt weld tested at a constant stress ratio R of 0.1. Here, w and t are the initial width and thickness of the specimen parallel cross-section (measured adjacent to the weld crown on the aluminium side of the joint),* F_{max} *and* F_{min} *are the maximum and minimum force being applied during testing and* N_f *is the number of cycles to failure. Included in the table are also the corresponding fracture location and fracture initiation point for each specimen.*

Specimen label	w **(mm)**	t **(mm)**	F_{max} **(N)**	F_{min} **(N)**	**Test frequency (Hz)**	N_f	**Fracture location**	**Fracture initiation point**
F1	6.02	3.95	4200	420	40	35152	Al-HAZ	face
F2	6.03	3.95	4800	480	30	25424	Al-HAZ	face
F3	6.01	4.01	3600	360	40	122930	EZ	root
F4	6.02	4.00	4800	480	30	5103	Close to Al/steel interface	defects
F5	6.01	4.01	3000	300	40	124859	Al-HAZ	face
F6	6.02	3.93	2400	240	50	775281	Al-HAZ	root
F7	6.02	3.94	2400	240	50	771270	Al-HAZ	root
F8	6.03	3.94	3000	300	40	147980	Al-HAZ	root
F9	6.02	3.94	3600	360	40	65804	Al-HAZ	root
F10	6.02	3.93	4200	420	40	22669	Al-HAZ	root
F11	6.02	3.94	2760	276	50	223984	Al-HAZ	root
F12	6.00	3.93	2760	276	50	277742	Al-HAZ	root

7 References

[1] Taub A, De Moor E, Luo A, Matlock DK, Speer JG, and Vaidya U, Materials for automotive lightweighting. Annu Rev Mater Res 2019;49:327-59. https://doi.org/10.1146/annurev-matsci-070218-010134.

[2] Goede M, Stehlin M, Rafflenbeul L, Kopp G, and Beeh E, Super Light Car—lightweight construction thanks to a multi-material design and function integration. Eur Transp Res Rev 2009;1(1):5-10. https://doi.org/10.1007/s12544-008-0001-2.

[3] Mallick PK, Materials, Design and Manufacturing for Lightweight Vehicles. New York: Woodhead Publishing; 2010.

[4] Joost WJ, Reducing Vehicle Weight and Improving U.S. Energy Efficiency Using Integrated Computational Materials Engineering. JOM 2012;64(9):1032-8. https://doi.org/10.1007/s11837-012-0424-z.

[5] Dilthey U and Stein L, Multimaterial car body design: challenge for welding and joining. Sci Technol Weld Join 2006;11(2):135-42. http://doi.org/10.1179/174329306x85967.

[6] Martinsen K, Hu SJ, and Carlson BE, Joining of dissimilar materials. CIRP Ann 2015;64(2): 679-99. https://doi.org/10.1016/j.cirp.2015.05.006.

[7] Cai W, Daehn G, Vivek A, Li J, Khan H, Mishra RS, et al., A state-of-the-art review on solid-state metal joining. J Manuf Sci Eng 2019;141(3):031012. https://doi.org/10.1115/1.4041182.

[8] AWS D8.14M:2008, Specification for Automotive Weld Quality - Arc Welding of Aluminum, American Welding Society, Miami, FL, 2008.

[9] Atabaki MM, Nikodinovski M, Chenier P, Ma J, Harooni M, and Kovacevic R, Welding of aluminum alloys to steels: an overview. J Manuf Sci Prod 2014;14(2):59-78. http://doi.org/10.1515/jmsp-2014-0007.

[10] Gullino A, Matteis P, and D'Aiuto F, Review of aluminum-to-steel welding technologies for car-body applications. Met 2019;9(3):315. https://doi.org/10.3390/met9030315.

[11] Borrisutthekul R, Mitsomwang P, Rattanachan S, and Mutoh Y, Feasibility of using TIG welding in dissimilar metals between steel/aluminum alloy. Energy Res J 2010;1(2):82-6. https://doi.org/10.3844/erjsp.2010.82.86.

[12] He H, Wu C, Lin S, and Yang C, Pulsed TIG Welding–Brazing of Aluminum–Stainless Steel with an Al-Cu Twin Hot Wire. J Mater Eng Perform 2019;28(2):1180-9. https://doi.org/10.1007/s11665-018-3848-y.

[13] Song J, Lin S, Yang C, Ma G, and Liu H, Spreading behavior and microstructure characteristics of dissimilar metals TIG welding–brazing of aluminum alloy to stainless steel. Mater Sci Eng A 2009;509(1-2):31-40. https://doi.org/10.1016/j.msea.2009.02.036.

[14] Qin G, Ji Y, Ma H, and Ao Z, Effect of modified flux on MIG arc brazing-fusion welding of aluminum alloy to steel butt joint. J Mater Process Technol 2017;245:115-21. https://doi.org/10.1016/j.jmatprotec.2017.02.022.

[15] Singh J, Arora KS, and Shukla DK, Dissimilar MIG-CMT weld-brazing of aluminium to steel: A review. J Alloy Compd 2019;783:753-64. https://doi.org/10.1016/j.jallcom.2018.12.336.

[16] Furukawa K, New CMT arc welding process–welding of steel to aluminium dissimilar metals and welding of super-thin aluminium sheets. Weld Int 2006;20(6):440-5. http://doi.org/10.1533/wint.2006.3598.

[17] Selvi S, Vishvaksenan A, and Rajasekar E, Cold metal transfer (CMT) technology - An overview. Def Technol 2018;14(1):28-44. https://doi.org/10.1016/j.dt.2017.08.002.

[18] Xu W, He H, Yi Y, Wang H, Yu C, and Fang W, Dissimilar joining of stainless steel and aluminum using twin-wire CMT. Weld World 2021:1-11. https://doi.org/10.1007/s40194-021-01089-0.

[19] Wang P, Chen X, Pan Q, Madigan B, and Long J, Laser welding dissimilar materials of aluminum to steel: an overview. Int J Adv Manuf Technol 2016;87(9):3081-90. https://doi.org/10.1007/s00170-016-8725-y.

[20] Sun J, Yan Q, Gao W, and Huang J, Investigation of laser welding on butt joints of Al/steel dissimilar materials. Mater Des 2015;83:120-8. https://doi.org/10.1016/j.matdes.2015.05.069.

[21] Möller B, Albrecht S, Wagener R, and Melz T, Fatigue Strength of Laser Beam Welded Steel-Aluminium Joints Considering Variable Amplitude Loading and Corrosive Environment. Procedia Struct Integr 2019. **18**: p. 556-569. https://doi.org/10.1016/j.prostr.2019.08.200.

[22] Hussein SA, Tahir ASM, and Hadzley AB, Characteristics of aluminum-to-steel joint made by friction stir welding: A review. Mater Today Commun 2015;5:32-49. https://doi.org/10.1016/j.mtcomm.2015.09.004.

[23] Watanabe T, Takayama H, and Yanagisawa A, Joining of aluminum alloy to steel by friction stir welding. J Mater Process Technol 2006;178(1):342-9. https://doi.org/10.1016/j.jmatprotec.2006.04.117.

[24] Ramachandran KK, Murugan N, and Shashi Kumar S, Performance analysis of dissimilar friction stir welded aluminium alloy AA5052 and HSLA steel butt joints using response surface method. Int J Adv Manuf Technol 2016;86(9):2373-92. https://doi.org/10.1007/s00170-016-8337-6.

[25] Springer H, Kostka A, Dos Santos J, and Raabe D, Influence of intermetallic phases and Kirkendall-porosity on the mechanical properties of joints between steel and aluminium alloys. Mater Sci Eng A 2011;528(13-14):4630-42. https://doi.org/10.1016/j.msea.2011.02.057.

[26] Wan L and Huang Y, Friction stir welding of dissimilar aluminum alloys and steels: a review. Int J Adv Manuf Technol 2018;99(5-8):1781-1811. https://doi.org/10.1007/s00170-018-2601-x.

[27] Haghshenas M and Gerlich AP, Joining of automotive sheet materials by friction-based welding methods: A review. Eng Sci Technol Int J 2018;21(1):130-48. https://doi.org/10.1016/j.jestch.2018.02.008.

[28] Fei X, Jin X, Peng N, Ye Y, Wu S, and Dai H, Effects of filling material and laser power on the formation of intermetallic compounds during laser-assisted friction stir butt welding of steel and aluminum alloys. Appl Phys A 2016;122(11):936. http://doi.org/10.1007/s00339-016-0462-4.

[29] Fei X, Jin X, Ye Y, Xiu T, and Yang H, Effect of pre-hole offset on the property of the joint during laser-assisted friction stir welding of dissimilar metals steel and aluminum alloys. Materi Sci Eng A 2016;653:43-52. https://doi.org/10.1016/j.msea.2015.11.101.

[30] Ozaki H and Kutsuna M, Dissimilar metal joining of zinc coated steel and aluminum alloy by laser roll welding. In: Kovacevic R, editor. Weld Process: IntechOpen 2012. https://doi.org/10.5772/48242.

[31] Thomy C and Vollertsen F, Laser-MIG hybrid welding of aluminium to steel—effect of process parameters on joint properties. Weld World 2012;56(5-6):124-32. https://doi.org/10.1007/BF03321356.

[32] Chen Y, Yang Z, Shi C, Xin Z, and Zeng Z, Laser-CMT Hybrid Welding-Brazing of Al/Steel Butt Joint: Weld Formation, Intermetallic Compounds, and Mechanical Properties. Mater 2019;12(22):3651. https://doi.org/10.3390/ma12223651.

[33] Chen S, Li S, Li Y, Huang J, Chen S, and Yang J, Butt welding-brazing of steel to aluminum by hybrid laser-CMT. J Mater Process Technol 2019;272:163-9. https://doi.org/10.1016/j.jmatprotec.2019.05.018.

[34] Ye Z, Huang J, Cheng Z, Gao W, Zhang Y, Chen S, et al., Combined effects of MIG and TIG arcs on weld appearance and interface properties in Al/steel double-sided butt welding-brazing. J Mater Process Technol 2017;250:25-34. https://doi.org/10.1016/j.jmatprotec.2017.07.003.

[35] Pouranvari M, Critical assessment 27: dissimilar resistance spot welding of aluminium/steel: challenges and opportunities. Mater Sci Technol 2017;33(15):1705-12. https://doi.org/10.1080/02670836.2017.1334310.

[36] Agudo L, Eyidi D, Schmaranzer CH, Arenholz E, Jank N, Bruckner J, et al., Intermetallic Fe_xAl_y-phases in a steel/Al-alloy fusion weld. J Mater Sci 2007;42(12):4205-14. https://doi.org/10.1007/s10853-006-0644-0.

[37] Lee W-B, Schmuecker M, Mercardo UA, Biallas G, and Jung S-B, Interfacial reaction in steel–aluminum joints made by friction stir welding. Scr Mater 2006;55(4):355-8. https://doi.org/10.1016/j.scriptamat.2006.04.028.

[38] Xia H, Zhao X, Tan C, Chen B, Song X, and Li L, Effect of Si content on the interfacial reactions in laser welded-brazed Al/steel dissimilar butted joint. J Mater Process Technol 2018;258:9-21. https://doi.org/10.1016/j.jmatprotec.2018.03.010.

[39] Li L, Xia H, Tan C, and Ma N, Influence of laser power on interfacial microstructure and mechanical properties of laser welded-brazed Al/steel dissimilar butted joint. J Manuf Process 2018;32:160-74. https://doi.org/10.1016/j.jmapro.2018.02.002.

[40] Meng Y, Gong M, Zhang S, Zhang Y, and Gao M, Effects of oscillating laser offset on microstructure and properties of dissimilar Al/steel butt-joint. Opt Lasers Eng 2020;128:106037. https://doi.org/10.1016/j.optlaseng.2020.106037.

[41] Li L, Xia H, Tan C, and Ma N, Effect of groove shape on laser welding-brazing Al to steel. J Mater Process Technol 2018;252:573-81. https://doi.org/10.1016/j.jmatprotec.2017.10.025.

[42] Xue J, Li Y, Chen H, and Zhu Z, Effects of heat input on wettability, interface microstructure and properties of Al/steel butt joint in laser-metal inert-gas hybrid welding-brazing. J Mater Process Technol 2018;255:47-54. https://doi.org/10.1016/j.jmatprotec.2017.11.063.

[43] Bang H, Bang H, Jeon G, Oh I, and Ro C, Gas tungsten arc welding assisted hybrid friction stir welding of dissimilar materials Al6061-T6 aluminum alloy and STS304 stainless steel. Mater Des 2012;37:48-55. https://doi.org/10.1016/j.matdes.2011.12.018.

[44] Ramachandran K, Murugan N, and Kumar SS, Effect of tool axis offset and geometry of tool pin profile on the characteristics of friction stir welded dissimilar joints of aluminum alloy AA5052 and HSLA steel. Mater Sci Eng A 2015;639:219-33. https://doi.org/10.1016/j.msea.2015.04.089.

[45] Ramachandran KK, Murugan N, and Kumar S, Friction Stir Welding of Aluminum Alloy AA5052 and HSLA Steel: Mechanical and microstructural characterization of dissimilar friction stir welded butt joints. Weld J 2015;94:291-300.

[46] Ghosh M, Gupta R, and Husain M, Friction stir welding of stainless steel to Al alloy: effect of thermal condition on weld nugget microstructure. Metall Mater Trans A 2014;45(2):854-63. http://doi.org/10.1007/s11661-013-2036-9.

[47] Kusuda Y, Honda develops robotized FSW technology to weld steel and aluminum and applied it to a mass-production vehicle. Industrial Robot: Int J 2013;40(3):208-12. https://doi.org/10.1108/01439911311309889.

[48] Grong Ø, Sandnes L, Bergh T, Vullum PE, Holmestad R, and Berto F, An analytical framework for modelling intermetallic compound (IMC) formation and optimising bond strength in aluminium-steel welds. Mater Des Process Commun 2019;1:e57. http://doi.org/10.1002/mdp2.57.

[49] Grong Ø, Sandnes L, and Berto F, A Status Report on the Hybrid Metal Extrusion & Bonding (HYB) Process and Its Applications. Mater Des Process Commun 2019;1(2):e41. http://doi.org/10.1002/mdp2.41.

[50] Leoni F, Grong Ø, Sandnes L, Welo T, and Berto F, Finite element modelling of the filler wire feeding in the hybrid metal extrusion & bonding (HYB) process. J Adv Join Process 2020;1:100006. https://doi.org/10.1016/j.jajp.2020.100006.

[51] Grong Ø, Recent advances in solid-state joining of aluminum. Weld J 2012;91(1):26-33.

[52] Aakenes UR, Grong Ø, and Austigard T, Application of the hybrid metal extrusion & bonding (HYB) method for joining of AA6082-T6 base material. Mater Sci Forum 2014;794:339-44. https://doi.org/10.4028/www.scientific.net/MSF.794-796.339.

[53] Grong Ø, Sandnes L, and Berto F, Progress in Solid State Joining of Metals and Alloys. Procedia Struct Integ 2019;17:788-98. https://doi.org/10.1016/j.prostr.2019.08.105.

[54] Sandnes L, Grong Ø, Torgersen J, Welo T, and Berto F, Exploring the hybrid metal extrusion and bonding process for butt welding of Al–Mg–Si alloys. Int J Adv Manuf Technol 2018;98(5):1059-65. http://doi.org/10.1007/s00170-018-2234-0.

[55] Sandnes L, Romere L, Berto F, Welo T, and Grong Ø, Assessment of the Mechanical Integrity of a 2 mm AA6060-T6 Butt Weld Produced Using the Hybrid Metal Extrusion & Bonding (HYB) Process – Part I: Bend Test Results. Procedia Manuf 2019;34:147-53. https://doi.org/10.1016/j.promfg.2019.06.132.

[56] Sandnes L, Romere L, Grong Ø, Berto F, and Welo T, Assessment of the Mechanical Integrity of a 2 mm AA6060-T6 Butt Weld Produced Using the Hybrid Metal Extrusion & Bonding (HYB) Process –

Part II: Tensile Test Results. Procedia Struct Integr 2019;17:632-42. https://doi.org/10.1016/j.prostr.2019.08.085.

[57] Sandnes L, Grong Ø, Welo T, and Berto F, Fatigue properties of AA6060-T6 butt welds made by hybrid metal extrusion & bonding. Fatigue Fract Eng Mater Struct 2020;43(10):2349-58. https://doi.org/10.1111/ffe.13302.

[58] Sandnes L, Rørvik G, Kulbotten IM, Grong Ø, and Berto F, Qualification of the hybrid metal extrusion & bonding (HYB) process for welding of aluminium offshore structures. Mater Des Process Commun 2020;e194. https://doi.org/10.1002/mdp2.194.

[59] Berto F, Sandnes L, Abbatinali F, Grong Ø, and Ferro P, Using the Hybrid Metal Extrusion & Bonding (HYB) Process for Dissimilar Joining of AA6082-T6 and S355. Procedia Struct Integr 2018;13:249-54. https://doi.org/10.1016/j.prostr.2018.12.042.

[60] Bergh T, Sandnes L, Johnstone D, Midgley PA, Berto F, Holmestad R, et al., Microstructural and mechanical characterisation of a hybrid metal extrusion & bonding aluminium-steel butt joint. Mater Charact 2020;173:110761. https://doi.org/10.1016/j.matchar.2020.110761.

[61] Sandnes L, Bergh T, Grong Ø, Holmestad R, Vullum PE, and Berto F, Interface Microstructure and Tensile Properties of a Third Generation Aluminium-Steel Butt Weld Produced Using the Hybrid Metal Extrusion & Bonding (HYB) Process. Mater Sci Eng A 2021;809:140975. https://doi.org/10.1016/j.msea.2021.140975.

[62] Coelho R, Kostka A, Dos Santos J, and Kaysser-Pyzalla A, Friction-stir dissimilar welding of aluminium alloy to high strength steels: Mechanical properties and their relation to microstructure. Mater Sci Eng A 2012;556:175-83. https://doi.org/10.1016/j.msea.2012.06.076.

[63] Okane M, Shitaka T, Ishida M, Chaki T, Yasui T, and Fukumoto M. Fatigue properties of butt welded aluminum alloy and carbon steel joints by friction stirring. J Phy: Conf Ser 2017;843:012040. https://doi.org/10.1088/1742-6596/843/1/012040.

[64] Yasui T, Tsubaki M, Fukumoto M, Shimoda Y, and Ishii T, High-speed weldability between 6063 and S45C by friction stir welding. Study of welding of dissimilar metals by friction stir welding (1st report). Weld Int 2006;20(4):284-9. https://doi.org/10.1533/wint.2006.3580.

[65] Karakizis P, Pantelis D, Dragatogiannis D, Bougiouri V, and Charitidis C, Study of friction stir butt welding between thin plates of AA5754 and mild steel for automotive applications. Int J Adv Manuf Technol 2019;102(9-12):3065-76. https://doi.org/10.1007/s00170-019-03388-9.

[66] Silvayeh Z, Domitner J, Sommitsch C, Hartmann M, Karner W, and Götzinger B, *Mechanical properties and fracture modes of thin butt-joined aluminum-steel blanks for automotive applications*. J Manuf Process, 2020. **59**: p. 456-467. https://doi.org/10.1016/j.jmapro.2020.09.050.

[67] Zhao S, Ni J, Wang G, Wang Y, Bi Q, Zhao Y, et al., Effects of tool geometry on friction stir welding of AA6061 to TRIP steel. J Mater Process Technol 2018;261:39-49. https://doi.org/10.1016/j.jmatprotec.2018.06.003.

[68] Leitao C, Arruti E, Aldanondo E, and Rodrigues DM, Aluminium-steel lap joining by multipass friction stir welding. Mater Des 2016;106:153-60. https://doi.org/10.1016/j.matdes.2016.05.101.

[69] Uematsu Y, Tokaji K, Tozaki Y, Nakashima Y, and Shimizu T, Fatigue behaviour of dissimilar friction stir spot welds between A6061-T6 and low carbon steel sheets welded by a scroll grooved tool without probe. Fatigue Fract Eng Mater Struct 2011;34(8):581-91. https://doi.org/10.1111/j.1460-2695.2010.01549.x.

[70] Ibrahim I, Uematsu Y, Kakiuchi T, Tozaki Y, and Mizutani Y, Fatigue behaviour of dissimilar Al alloy/galvanised steel friction stir spot welds fabricated by scroll grooved tool without probe. Sci Technol Weld Join 2015;20(8):670-8. https://doi.org/10.1179/1362171815Y.0000000053.

[71] Rao HM, Kang J, Shi L, Sigler DR, and Carlson BE, Effect of specimen configuration on fatigue properties of dissimilar aluminum to steel resistance spot welds. Int J Fatigue 2018;116:13-21. https://doi.org/10.1016/j.ijfatigue.2018.06.009.

[72] Geng H, Sun L, Li G, Cui J, Huang L, and Xu Z, Fatigue fracture properties of magnetic pulse welded dissimilar Al-Fe lap joints. Int J Fatigue 2019;121:146-54. https://doi.org/10.1016/j.ijfatigue.2018.12.027.

[73] Ling Z, Li Y, Luo Z, Ao S, Yin Z, Gu Y, et al., Microstructure and fatigue behavior of resistance element welded dissimilar joints of DP780 dual-phase steel to 6061-T6 aluminum alloy. Int J Adv Manuf Technol 2017;92(5):1923-31. https://doi.org/10.1007/s00170-017-0310-5.

[74] Mirza FA, Macwan A, Bhole SD, Chen DL, and Chen XG, Microstructure, tensile and fatigue properties of ultrasonic spot welded aluminum to galvanized high-strength-low-alloy and low-carbon steel sheets. Mater Sci Eng A 2017;690:323-36. https://doi.org/10.1016/j.msea.2017.03.023.

[75] Macwan A, Kumar A, and Chen DL, Ultrasonic spot welded 6111-T4 aluminum alloy to galvanized high-strength low-alloy steel: Microstructure and mechanical properties. Mater Des 2017;113:284-96. https://doi.org/10.1016/j.matdes.2016.10.025.

[76] Uematsu Y, Kakiuchi T, Tozaki Y, and Kojin H, Comparative study of fatigue behaviour in dissimilar Al alloy/steel and Mg alloy/steel friction stir spot welds fabricated by scroll grooved tool without probe. Sci Technol Weld Join 2012;17(5):348-56. https://doi.org/10.1179/1362171812Y.0000000014.

[77] Tran VX and Pan J, Fatigue behavior of dissimilar spot friction welds in lap-shear and cross-tension specimens of aluminum and steel sheets. Int J Fatigue 2010;32(7):1167-79. https://doi.org/10.1016/j.ijfatigue.2009.12.011.

[78] Uematsu Y, Kakiuchi T, Kondoh E, Tozaki Y, and Ibrahim I, Fatigue behavior of dissimilar A6061/rolled steel (SS400) friction stir welds. J Jpn Weld Soc 2013;31:112-8. https://doi.org/10.2207/qjjws.31.112.

[79] Uzun H, Dalle Donne C, Argagnotto A, Ghidini T, and Gambaro C, Friction stir welding of dissimilar Al 6013-T4 To X5CrNi18-10 stainless steel. Mater Des 2005;26(1):41-6. https://doi.org/10.1016/j.matdes.2004.04.002.

[80] Grong Ø, Sandnes L, Ferro P, and Berto F, Hybrid Metal Extrusion and Bonding. In de Basto Pereira AM and da Silva FJG, Editors. Handbook of Welding: Processes, Control and Simulations, NOVA Science publisher, New York, 2021 (in press).

[81] ASTM E466-15, Standard Practice for Conducting Force Controlled Constant Amplitude Axial Fatigue Tests of Metallic Materials. ASTM International, West Conshohocken, PA, 2015.

[82] Zerbst U and Hensel J, Application of fracture mechanics to weld fatigue. Int J Fatigue 2020;139: 105801. https://doi.org/10.1016/j.ijfatigue.2020.105801.

[83] Leoni F, Sandnes L, Grong Ø, and Berto F, Mechanical testing of gas metal arc AA6082-T6 weldments. Mater Des Process Commun 2020;e160. https://doi.org/10.1002/mdp2.160.

[84] Mazzolani FM, *Aluminium alloy structures*. 2nd ed. 1995, London: E & FN Spon.

[85] G. E. Dieter DB, *Mechanical Metallurgy*. 1988, London: McGraw-Hill.

[86] ASTM E739-10(2015), Standard Practice for Statistical Analysis of Linear or Linearized Stress-Life (S-N) and Strain-Life (ε-N) Fatigue Data. ASTM International, West Conshohocken, PA, 2015.

[87] EN-1999. Eurocode 9: Design of aluminium structures—Part 1-3: structures susceptible to fatigue. European Committee for Standardization, 1999 (2007).

[88] Ma M, Lai R, Qin J, Wang B, Liu H, and Yi D, Effect of weld reinforcement on tensile and fatigue properties of 5083 aluminum metal inert gas (MIG) welded joint: Experiments and numerical simulations. Int J Fatigue 2021;144:106046. https://doi.org/10.1016/j.ijfatigue.2020.106046.

[89] Schork B, Zerbst U, Kiyak Y, Kaffenberger M, Madia M, and Oechsner M, Effect of the parameters of weld toe geometry on the FAT class as obtained by means of fracture mechanics-based simulations. Weld World 2020;64(6):925-36. https://doi.org/10.1007/s40194-020-00874-7.

[90] Hobbacher AF, The new IIW recommendations for fatigue assessment of welded joints and components – A comprehensive code recently updated. Int J Fatigue 2009;31(1):50-8. https://doi.org/10.1016/j.ijfatigue.2008.04.002.

[91] Hobbacher A, Recommendations for fatigue design of welded joints and components. 2nd ed. Springer International Publishing; 2016.

[92] da Silva J, Costa JM, Loureiro A, and Ferreira JM, Fatigue behaviour of AA6082-T6 MIG welded butt joints improved by friction stir processing. Mater Des 2013;51:315-22. https://doi.org/10.1016/j.matdes.2013.04.026.

[93] Moreira P, Richter-Trummer V, and de Castro P, Fatigue Behaviour of FS, LB and MIG Welds of AA6061-T6 and AA6082-T6. In Shi GC, editor. Multiscale fatigue crack initiation and propagation of engineering materials: structural integrity and microstructural worthiness, Springer. 2008:85-111.

[94] Cirello A, Buffa G, Fratini L, and Pasta S, AA6082-T6 friction stir welded joints fatigue resistance: influence of process parameters. Proc Inst Mech Eng Part B: J Eng Manuf 2006;220(6):805-11. http://doi.org/10.1243/09544054JEM319.

[95] Costa J, Ferreira J, and Borrego L, Influence of spectrum loading on fatigue resistance of AA6082 friction stir welds. Int J Struct Integr 2011;2:122-34. https://doi.org/10.1108/17579861111135888.

Highlights

- Al-steel HYB butt joint exhibits unique fatigue properties in as-welded condition
- Interfacial cracking is prevented by a high intrinsic Al-Fe bond strength
- Fatigue crack development occurs at the weld toe on the Al side of the joint
- Joint fatigue strength is comparable with that of corresponding Al-Al weldments

Declaration of interests

☒ The authors declare that they have no known competing financial interests or personal relationships that could have appeared to influence the work reported in this paper.

☐The authors declare the following financial interests/personal relationships which may be considered as potential competing interests: